arXiv:0706.3306v1 [physics.atom-ph] 22 Jun 2007

Theoretical studies of high-harmonic generation: Effects of symmetry, degeneracy and orientation.

C. B. Madsen and L. B. Madsen
Lundbeck Foundation Theoretical Center for Quantum System Research,
Department of Physics and Astronomy, University of Aarhus, 8000 Aarhus C, Denmark.

(Dated: February 1, 2008)

Using a quantum mechanical three-step model we present numerical calculations on the high-harmonic generation from four polyatomic molecules. Ethylene (C_2H_4) serves as an example where orbital symmetry directly affects the harmonic yield. We treat the case of methane (CH_4) to address the high-harmonic generation resulting from a molecule with degenerate orbitals. To this end we illustrate how the single orbital contributions show up in the total high-harmonic signal. This example illustrates the importance of adding coherently amplitude contributions from the individual degenerate orbitals. Finally, we study the high-harmonic generation from propane (C_3H_8) and butane (C_4H_{10}). These two molecules, being extended and far from spherical in structure, produce harmonics with non-trivial orientational dependencies. In particular, propane can be oriented so that very high-frequency harmonics are favorized, and thus the molecule contains prospects for the generation of UV attosecond pulses.

PACS numbers: 42.65.Ky,33.80.Rv

I. INTRODUCTION

In the process of high-harmonic generation (HHG) high-frequency coherent radiation is emitted from an atom or molecule when exposed to intense femtosecond laser light. This process has been the subject of extensive studies during the last couple of decades due to possible applications, including, e.g., generation of coherent UV attosecond pulses [1, 2, 3], carrier-envelope phase retrieval [4] and tomographic reconstruction of molecular orbitals [5, 6, 7].

Whereas early HHG studies focused on atomic systems, it was not until the new millennium that experimental work on molecules gathered pace. Studies on HHG from molecules is motivated by the expectation that the more degrees of freedom and non-spherical symmetry as compared to atoms may lead to richer physics and a higher degree of control. Hitherto the molecules considered have mostly been diatomic or linear systems and it is only just recently that experimental results on HHG from more complicated molecules have become available [8]. Here we apply a quantum mechanical three-step model to investigate theoretically HHG from polyatomic molecules of current interest to experimentalists [6, 8]. In our theory, we use a detailed description of the molecular orbitals, obtained from Hartree-Fock calculations. We illustrate the effect of orbital symmetry on HHG by studying the orientation dependence of the harmonic signal from ethylene (C_2H_4). The methane molecule (CH_4) is used to demonstrate how degenerate HOMOs influence the harmonic spectrum. In particular, we show the importance of including coherently the contribution from every single HOMO when calculating the harmonic yield from an oriented molecule. We demonstrate how the extended and non-spherical molecules propane (C_3H_8) and butane (C_4H_{10}) give rise to harmonic spectra with a rather complex orientational dependence. In the case of propane harmonics near the cutoff can be selected by orienting the molecule, and since we expect such harmonics to be synchronically emitted [9] orientation of propane is identified as a tool for generating attosecond pulses. It is the first time, to our knowledge, an investigation of the detailed orientational dependence of the single molecule high-harmonic signal from such complex systems is presented.

The paper is organized as follows. In Sec. II we derive formulas for the single-particle respons from a system with degenerate HOMOs, and we review the quantum mechanical three-step model used to calculate the harmonic yield [10]. In Sec. III we briefly discuss some numerical details for our calculations. Section IV contains numerical results describing the harmonic yield from each of the aforementioned molecules. Especially, we treat several effects related to the orientation of such systems. Finally, we give a summary and the conclusions in Sec. V. [We use atomic units ($e = \hbar = m_e = a_0 = 1$) throughout.]

II. THEORY

A. Harmonic yield from a statistical mixture of molecules

The complex amplitude for the emission of harmonics with frequency ω_{HHG} polarized along the linear polarization vector $\boldsymbol{e}$ is obtained from the Fourier transform of the dipole acceleration

$$A_{\boldsymbol{e}}(\omega_{\mathrm{HHG}}) = \boldsymbol{e} \cdot \int dt\, e^{-i\omega_{\mathrm{HHG}} t} \frac{d^2}{dt^2} \langle \hat{\boldsymbol{d}} \rangle (t), \qquad (1)$$

where $\langle \hat{\boldsymbol{d}} \rangle (t)$ is the expectation value of the dipole operator $\hat{\boldsymbol{d}}$ of the molecule. The corresponding power density is given by [11, 12]:

$$S_{\boldsymbol{e}}(\omega_{\mathrm{HHG}}) \propto |A_{\boldsymbol{e}}(\omega_{\mathrm{HHG}})|^2. \tag{2}$$

The quantum state will be a mixed state, since several unobserved variables appear in a measurement of the harmonic signal. First, typically several electrons from a given molecule will contribute significantly to the HHG because of degeneracy of the highest occupied molecular orbital (HOMO). An experiment recording the total harmonic yield from an ensemble of ground state molecules cannot distinguish contributions from the individual degenerate HOMOs. Second, since perfect orientation of molecules is unrealistic, the measured harmonic yield arises from an ensemble of molecules with different orientations. In this section we treat these unresolved degrees of freedom, using and elaborating the results of recent work [13]. Initially, the molecule is in a stationary thermal state at temperature T, and the system is completely characterized by the density matrix $\hat{\rho}_0 = \exp(-\hat{H}/k_B T)/Z$, with partition function $Z = \mathrm{Tr}[\exp(-\hat{H}/k_B T)]$, $\hat{H}$ the field-free molecular Hamiltonian and k_B Boltzmann's constant. We want to resolve the molecular initial state on energy eigenstates. The molecules we consider are, however, so complex that several simplifying assumptions have to be made in order to obtain a practical theoretical formulation. According to the Born-Oppenheimer approximation, we can separate the electron and nuclear motion, and we will assume only the electronic ground state be populated. Next we adapt the single-active-electron (SAE) approximation, and introduce an index λ in order to be able to discriminate between the degenerate HOMOs of this active electron. The nuclear motion consists of rotation and vibration. We shall assume that only the vibrational groundstate is occupied, whereas the rotation needs to be treated in more detail to take account of an oriented molecule. In doing so, we neglect the rovibrational interaction such that rotation and vibration can be treated separately. The rotation is characterized by the asymmetric top quantum numbers J, τ and M [14]. We may, accordingly, specify the energy eigenstates by their electronic and rotational degrees of freedom, $|\lambda\rangle \otimes |J\tau M\rangle$. When the system interacts with a laser, the energy eigenstates will evolve according to a unitary operator that describes any number of orienting pump pulses followed by a short, intense laser pulse that drives the HHG [spontaneous decay processes can be neglected on the timescales we consider]. The orientation pulses are not strong enough to affect the electronic motion appreciably [15], while the nuclear dynamic can be considered as frozen during the short high-harmonic generating pulse [13]. Thus, if the delay between the final orienting pulse and the driving pulse is denoted by t_d, we can split the time evolution operator according to $U(t) \simeq U_{\mathrm{HHG}}(t) \otimes U_{\mathrm{orient}}(t_d)$ for a description of the evolution when the HHG is produced, where $U_{\mathrm{HHG}}(t)$ propagates the electronic part of the molecular state during the pulse of the driving laser and $U_{\mathrm{orient}}(t_d)$ accounts for the evolution of the rotational state of the molecule. The energy eigenstates then evolve as follows

$$\begin{aligned} |\Psi^\lambda_{J\tau M}(t)\rangle &\simeq (U_{\mathrm{HHG}}(t)|\lambda\rangle) \otimes (U_{\mathrm{orient}}(t_d)|J\tau M\rangle) \\ &= |\psi_\lambda(t)\Phi_{J\tau M}(t_d)\rangle. \end{aligned} \tag{3}$$

We return to the time evolution of the system in Sec. II B. Our current goal is to calculate the expectation value of the dipole operator as this enters Eqs. (1) and (2). This evaluation is most conveniently done by expanding the energy eigenstates in the position basis $|\boldsymbol{r}, \phi, \theta, \chi\rangle$ in which the dipole operator is diagonal

$$\langle \hat{\boldsymbol{d}}(t)\rangle = \mathrm{Tr}\left[\hat{\rho}(t)\hat{\boldsymbol{d}}\right] = \mathrm{Tr}\left[U(t)\hat{\rho}_0 U^\dagger(t)\hat{\boldsymbol{d}}\right] \simeq \int_0^{2\pi} d\phi \int_0^{\pi} d\theta \sin\theta \int_0^{2\pi} d\chi G_{t_d}(\phi,\theta,\chi) \sum_\lambda \langle \hat{\boldsymbol{d}}_\lambda\rangle(\phi,\theta,\chi,t) \tag{4}$$

with

$$\begin{aligned} \langle \hat{\boldsymbol{d}}_\lambda\rangle(\phi,\theta,\chi,t) &= \int d\boldsymbol{r} |\psi_\lambda(\boldsymbol{r},\phi,\theta,\chi,t)|^2 \hat{\boldsymbol{d}}, & (5) \\ G_{t_d}(\phi,\theta,\chi) &= \sum_{J,\tau,M} P_{J\tau} |\Phi_{J\tau M}(\phi,\theta,\chi;t_d)|^2, & (6) \end{aligned}$$

and $P_{J\tau} = \exp(-E_{J\tau}/k_B T)$ the Boltzmann weight of the asymmetric top wavefunction $\langle \phi,\theta,\chi|U_{\mathrm{orient}}(t_d)|J\tau M\rangle = \Phi_{J\tau M}(\phi,\theta,\chi;t_d)$ of energy $E_{J\tau}$.

Consequently, using Eqs. (1) and (2), the harmonic signal is given by

$$\begin{aligned} S_{\boldsymbol{e}}(\omega_{\mathrm{HHG}}) \propto \Bigg| \sum_\lambda \int_0^{2\pi} d\phi \int_0^{\pi} d\theta \sin\theta \int_0^{2\pi} d\chi \\ \times G_{t_d}(\phi,\theta,\chi) A^\lambda_{\boldsymbol{e}}(\omega_{\mathrm{HHG}},\phi,\theta,\chi) \Bigg|^2 \end{aligned} \tag{7}$$

with

$$A^\lambda_{\boldsymbol{e}}(\omega_{\mathrm{HHG}},\phi,\theta,\chi) = \boldsymbol{e} \cdot \int dt\, e^{-i\omega_{\mathrm{HHG}} t} \frac{d^2}{dt^2} \langle \hat{\boldsymbol{d}}_\lambda\rangle(\phi,\theta,\chi). \tag{8}$$

In general, the degenerate HOMOs will interfere due to the coherent sum over λ in Eq. (7). Nevertheless, there are special cases where the degeneracy enters simply as a factor multiplying the signal from a single HOMO. For example we mention that if the degeneracy is due to spin multiplicity, N_{S}, the sum over different HOMOs yields a factor N_{S}^2 in the signal. Another instance occurs when the HOMOs differ simply by a rotation. Then, in the case of a randomly oriented ensemble of molecules, i.e., $G_{t_d} = 1/(8\pi^2)$, it is obvious that HOMOs must each give rise to the same complex number when the single HOMO amplitude, $A^\lambda_{\boldsymbol{e}}(\omega_{\mathrm{HHG}},\phi,\theta,\chi)$, is averaged over all orientations. It then follows from Eq. (7) that the degeneracy will again enter as a factor multiplying the signal from a single HOMO.

B. Model

As described in the previous section the system starts out in a statistically mixed state composed of the energy eigenstates. Each $|\lambda\rangle \otimes |J\tau M\rangle$ state evolves according to Eq. (3). In this section we focus on the time evolution of the system.

First, propagating the asymmetric top energy eigenstates, $|J\tau M\rangle$, to obtain the $|\Phi_{J\tau M}(t_d)\rangle$'s at the time t_d of the high-harmonic probing pulse is a numerically demanding task. The issue has already been addressed in several studies [15, 16, 17], and in the present work, we will assume either G_{t_d} to be simply uniform (no preferred orientation) or use an idealized orientational distribution to be specified in Sec. IV.

Next, we focus on the electronic part of the time evolution. In the field-free initial state the HOMO wave function is conveniently expressed in a spherical expansion in the body fixed (BF) frame

$$\psi_\lambda^{\mathrm{BF}}(\boldsymbol{r}) = \sum_{l,m} F_{l,m}^{\lambda}(r) Y_l^m(\hat{\boldsymbol{r}}). \tag{9}$$

Asymptotically this expression must follow the Coulomb form

$$\psi_\lambda^{\mathrm{BF}}(\boldsymbol{r}) \sim \sum_{l,m} C_{l,m}^{\lambda} r^{\mathcal{Z}/\kappa - 1} \exp(-\kappa r) Y_l^m(\hat{\boldsymbol{r}}) \tag{10}$$

with $\kappa = \sqrt{2I_P}$, I_P the ionization potential, $\mathcal{Z}$ the net charge of the molecule when the HOMO electron is removed and where the $C_{l,m}^{\lambda}$'s are fitting coefficients. More detail on how to obtain wavefunctions in Eqs. (9) and (10) is given in Sec. III. We wish to carry out calculations in a laboratory fixed (LF) system defined by the laser polarization, and for a molecule of arbitrary orientation LF and BF coordinate axes do not in general coincide. Hence, we rotate the BF wave function to obtain the LF wave function by application of the rotation operator

$$\psi_\lambda^{\mathrm{LF}}(\boldsymbol{r}, \phi, \theta, \chi) = \hat{D}(\phi, \theta, \chi) \psi_\lambda^{\mathrm{BF}}(\boldsymbol{r}), \tag{11}$$

where the rotation is given by the Euler angles ϕ, θ and χ. Following the conventions of [14] θ is the angle between the BF z-axis and the LF Z-axis, ϕ denotes a rotation around the Z-axis, and finally χ denotes a rotation around the z-axis. Note that the effect of $\hat{D}$ is readily evaluated in the spherical harmonic basis used in Eqs. (9) and (10) [14].

We consider the case where the driving laser pulse contains several cycles such that a Floquet approach is suitable. Hence using the Coulomb gauge and the dipole approximation, a laser field with frequency ω and period $T = 2\pi/\omega$ is described by the vector potential $\boldsymbol{A}(t) = \boldsymbol{A}_0 \cos(\omega t)$. According to the quantum mechanical three-step model described in [18] for atoms and [10] for molecules the electronic time evolution, given by $U_{\mathrm{HHG}}(t)$ [see Eq. (3)], consists of a HOMO electron being transfered to the continuum via above threshold ionization (ATI), i.e., by absorbing a number of photons from the driving laser. The electron then propagates in the laser-dressed continuum and is eventually, due to the periodicity of the laser field, driven back to a recombination with the molecule, where it returns to the HOMO. Within this model the complex amplitude for the emission of harmonics polarized along the unit vector $\boldsymbol{e}$ with frequency $\omega_{\mathrm{HHG}}^N = N\omega$ (N integer) is [10]

$$A_{\boldsymbol{e}}^{\lambda}(\omega_{\mathrm{HHG}}^N, \phi, \theta, \chi) \propto \sum_{l_2, l_1} \sum_{m_2', m_1'} \sum_{m_2, m_1} D_{m_2', m_2}^{l_2 *}(\phi, \theta, \chi) D_{m_1', m_1}^{l_1}(\phi, \theta, \chi) C_{l_1, m_1}^{\lambda} \sum_{k} \sum_{C(k)} B_{l_2, m_2', m_2}^{\lambda, N, k, \boldsymbol{e}}(C(k)) A_{l_1, m_1'}^{k}(C(k)). \tag{12}$$

Here $D_{m_i', m_i}^{l}(\phi, \theta, \chi)$ with $i = 1, 2$ is the Wigner rotation function [14], while

$$C_{l_1, m_1}^{\lambda} A_{l_1, m_1'}^{k}(C(k)) = -C_{l_1, m_1}^{\lambda} \frac{1}{T} \Gamma\left(1 + \frac{\mathcal{Z}/\kappa}{2}\right) 2^{\frac{\mathcal{Z}/\kappa}{2}} \kappa^{\mathcal{Z}/\kappa} (\pm 1)^{l_1} \frac{\exp[iS(t'_{C(k)})]}{\sqrt{[-iS''(t'_{C(k)})]^{1+\mathcal{Z}/\kappa}}} Y_{l_1}^{m_1'}(\hat{\boldsymbol{q}}') \Big|_{\boldsymbol{q}' = \boldsymbol{K}_k + \boldsymbol{A}(t'_{C(k)})} \tag{13}$$

and

$$B_{l_2, m_2', m_2}^{\lambda, N, k, \boldsymbol{e}}(C(k)) = i \frac{(2\pi)^2}{T} \int_0^T dt \frac{\exp[i(N\omega t - S(t))]}{L_0(t, t'_{C(k)})} (\boldsymbol{e} \cdot \boldsymbol{\nabla}_{\boldsymbol{q}}) \left[\tilde{F}_{l_2, m_2}^{\lambda}(q) Y_{l_2}^{m_2'}(\hat{\boldsymbol{q}})\right]^* \Big|_{\boldsymbol{q} = \boldsymbol{K}_k + \boldsymbol{A}(t)}, \tag{14}$$

along with their Wigner rotation functions, are interpreted as ATI and propagation-recombination amplitudes, respectively, of a HOMO electron having absorbed k photons during the ATI-step. In Eqs. (13) and (14) $\boldsymbol{q}$

and $\boldsymbol{q}'$ are electron momenta and

$$S(t) = k\omega t + \boldsymbol{K}_k \cdot \frac{\boldsymbol{A}_0}{\omega}\sin(\omega t) + \frac{U_p}{2\omega}\sin(2\omega t) \qquad (15)$$

is the quasi-classical action. The index $C(k)$ in Eqs. (12)-(14) denotes the saddle-points. For each k the saddle-points $t'_{C(k)}$ are defined by the condition $S'(t'_{C(k)}) = 0$, and we use the ones with $0 \leq \mathrm{Re}(t'_{C(k)}) < T$ along with $\mathrm{Im}(t'_{C(k)}) > 0$. The factor $(\pm 1)^{l_1}$ in Eq. (13) corresponds to the limits $\pm i\kappa$ of the size q' of the electron momentum at the saddle-points. The factor $1/L_0(t, t'_{C(k)}) = \sigma\alpha_0(\sin\omega t'_{C(k)} - \sin\omega t)$ in Eq. (14), with $\sigma = \pm 1$ to assure $\mathrm{Re}(L_0) > 0$, describes the decrease of the amplitude of the electron wave as it propagates in the field-dressed continuum. Also, $\boldsymbol{K}_k$ is the part of the continuum electron momentum arising from absorption of k laser photons during ATI, thus $K_k = \sqrt{2(k\omega - I_p - U_p)}$ with $U_p = A_0^2/4$ the ponderomotive potential and $\boldsymbol{e}_{\boldsymbol{K}_k} = \sigma\boldsymbol{e}_{\boldsymbol{A}_0}$. Finally, in Eq. (14) the function $\tilde{F}^{\lambda}_{l_2,m_2}(q)$ is the radial part of the momentum space HOMO wave function, obtained by taking the Fourier transform of Eq. (11) (see [10] for further details).

III. CALCULATIONAL DETAILS

We have determined the Hartee-Fock wave functions for ethylene (C_2H_4), methane (CH_4), propane (C_3H_8) and butane (C_4H_{10}) in a spherical basis along with the asymptotic coefficients using the technique described in [19]. In Table I we list the ionization potentials I_p and the asymptotic $C^{\lambda}_{l,m}$-coefficients entering Eq. (10). Note that the results in the case of ethylene differ from those in [19] because our choice of the BF axes in the present work follows the convention of [16] with the xz-plane coinciding with the molecular plane, whereas in [19] the molecular plane was chosen to coincide with the yz-plane.

IV. RESULTS AND DISCUSSION

In this section we present results on the high-harmonic yield from ethylene, methane, propane and butane. Since we do not include effects of propagation [22, 23] our calculations cannot be directly compared with the experimental results of Ref. [8]. If our main purpose was the optimization of the harmonic yield with the object of generating attosecond pulses then, surely, phase-matching should be taken into account. Nevertheless, in this theoretical work aiming at isolating and illustrating clearly the effects of symmetry, degenerate orbitals and orientation, we find it reasonable to disregard phase-matching: first, because propagation effects can be reduced experimentally by using a gas jet which is short compared to the coherence length [24], and second, an understanding of the single molecular response is needed in order to understand the harmonic yield from a whole gas of molecules.

In all results presented below, we calculate the signal of harmonics polarized along a linearly polarized 800 nm, 1.8×10^{14} W/cm^2 driving laser. As the light is linearly polarized the results are independent of ϕ, the rotation around the polarization vector. We consider molecules that are either randomly oriented or have been one- or three-dimensionally oriented. The orientational distributions G_{t_d} [see Eqs. (6)-(7)] corresponding to random, one-dimensional or three-dimensional orientation are as follows

$$\begin{aligned} G^{\mathrm{random}}_{t_d} &= \frac{1}{8\pi^2}, && (16)\\ G^{\mathrm{1D}}_{t_d}(\theta',\chi') &= \frac{1}{4\pi^2}\frac{\delta(\theta'-\theta)}{\sin\theta'}, && (17)\\ G^{\mathrm{3D}}_{t_d}(\theta',\chi') &= \frac{1}{2\pi}\frac{\delta(\theta'-\theta)}{\sin\theta'}\delta(\chi'-\chi). && (18) \end{aligned}$$

Here the BF z-axis is oriented at angle θ with respect to the LF Z-axis in the cases of one- and three-dimensional orientation and the molecule is rotated an angle χ around the BF z-axis in the case of three-dimensional orientation.

A. Ethylene: Effects of the orbital symmetry

We first present results on the HHG from ehtylene (C_2H_4). This molecule has a non-degenerate HOMO which makes the influence of the HOMO on the harmonic signal relatively transparent. Additionally, ethylene is interesting from the point of view that field-free one-dimensional alignment has been carried out experimentally [16] and field-free three-dimensional alignment has been explored theoretically [17]. Consequently, the theoretical results presented below may, in principle, be subject to experimental investigations.

Figure 1 shows HHG spectra from ethylene at different orientations corresponding to the orientational distributions of Eqs. (16) and (17). The overall effect of orienting the molecule is a scaling of the spectrum. The reason for this scaling is that all harmonics have similar orientational dependence. We also note the absence of even harmonics in the spectrum, which is easily explained from the inversion symmetry of the HOMO of ethylene: The inversion symmetry means that the HOMO is composed of angular momentum states separated by even multiples of $\hbar$ (see Table I). At the same time absorption and emission of laser photons change the size of the electronic orbital angular momentum by $\pm\hbar$, so in order both to start off and end up in one of the angular momentum states of the HOMO an even number of dipole transitions is necessary. Hence, the HHG process requires the absorption of an odd number of photons followed by the emission of a single odd harmonic.

We have investigated HHG from C_2H_4 that has been fixed in both θ- and χ-angles corresponding to the three-

TABLE I: The molecular properties of the alkalenes used in this work for evaluation of HHG. I_p is the experimental adiabatic ionization potential [20]. The remaining numbers in the table give the values of the asymptotic coefficients, $C^{\lambda}_{l,m}$, entering Eq. (10) based on GAMESS calculation [21] using a triple zeta valence basis set with diffuse sp shells. The three degenerate HOMOs in CH_4 are denoted by HOMO1, HOMO2 and HOMO3.

		C_2H_4		CH_4		C_3 H_8	C_4H_{10}
		HOMO	HOMO1	HOMO2	HOMO3	HOMO	HOMO
I_P (eV)		10.5	12.6	12.6	12.6	10.9	10.6
l	m						
0	0						2.24
1	0				-1.65		
1	±1	$-1.09i$	±1.16	$-1.16i$		±0.36	
2	0						-1.87
2	±1		$0.36i$	±0.36		∓0.70	
2	±2				$\pm0.36i$		$-3.15 \mp 0.15i$
3	0				0.15		
3	±1	$-0.23i$	±0.07	$-0.07i$		∓0.21	
3	±3		∓0.09	$-0.09i$		∓0.54	
4	0						0.99
4	±2						1.14
4	±4						1.94
4	±3					±0.20	
5	±3					∓0.06	
6	0						-0.28
6	±2						-0.28
6	±4						-0.31
6	±6						-0.46

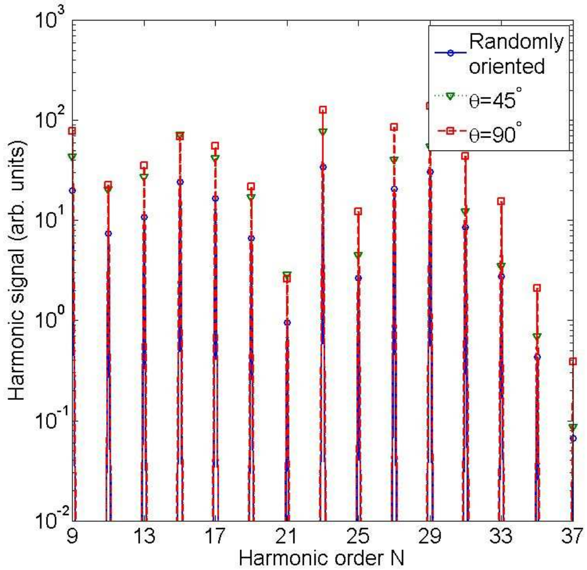

FIG. 1: (Color online) The orientational dependence of the harmonic spectrum from ethylene. The absence of even harmonics is explained by the inversion symmetry of the HOMO (see text).

dimensional orientation given by Eq. (18). Figure 2 shows representative results of the calculations. In order to understand the results, we also show the HOMO of ethylene in the figure. The meaning of the Euler angles was explained below Eq. (9). In the model used to simulate HHG an electron has to escape along the laser polarization axis [cf. Eq. (13)]. This is impossible, if the polarization axis lies along the nodal plane, which is the reason for the vanishing harmonic signal, when either $\theta = 0^\circ$ (180°) or $\chi = 0^\circ$ $(180^\circ, 360^\circ)$. When the molecule is rotated the nodal plane is removed from the polarization axis of the laser and the strength of the harmonics increases. As seen from Figs. 2(b) and (c) the harmonics peak at different values of the Euler angle θ. The varying positions of the peaks arise from different orientational behavior of the ionization and propagation-recombination steps making up the HHG process [cf. the discussion below Eq. (12)-(14)]: As the electron escapes along the polarization direction the ionization is maximal when θ lies in between 0° and 90° [19]. The propagation-recombination step, however, is optimized when $\theta = 90^\circ$, but the width of the peak depends on the harmonic order. These observations account for the different orientational behavior of the harmonics shown on Figs. 2(b) and (c).

We note, in passing, that a set of data as the ones presented in Figs. 2(b) and (c) for a full range of harmonic energies would, in principle, allow a tomographic reconstruction of the HOMO [5].

B. Methane: Interference of degenerate HOMOs

We now turn to the harmonic yield from the methane molecule (CH_4). Methane has three degenerate HOMOs

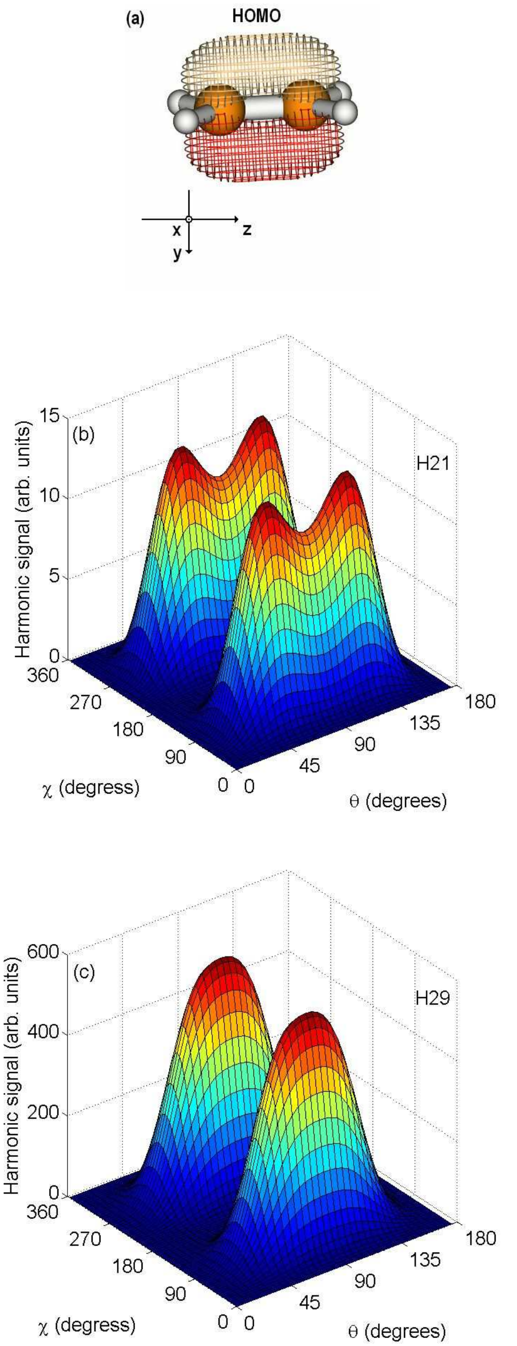

FIG. 2: (Color online) The orientational dependencies of the harmonics reflect the HOMO of ethylene. In particular the harmonics vanish, when the laser polarization coincides with the nodal plane of the HOMO. Panel (a) shows the geometry of ethylene (C_2H_4) along with an isocontour for the HOMO. Dark shading (red online) denotes a negative sign of the HOMO wave function. Light shading (brownish online) denotes a positive sign. Directions of the BF axes are shown. We always choose the center of mass as the origin of the BF coordinate system. Panels (b) and (c) present the dependencies of the 21st (H21) and 29th (H29) harmonics on orientation as given by Euler angles θ and χ.

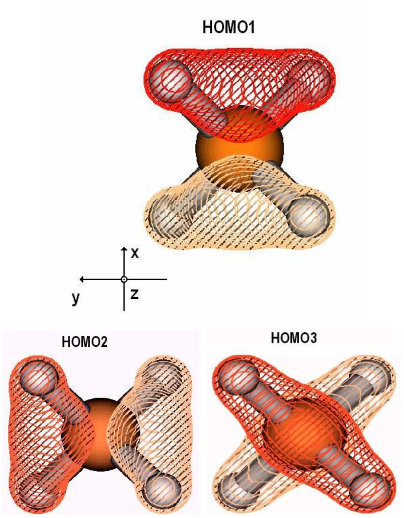

FIG. 3: (Color online) The geometry of the methane molecule (CH_4) along with isocontours of the three degenerate HOMOs. The signs of the HOMO wave functions are indicated by the coloring, where dark shading (red online) denotes a negative sign and a light shading (brownish online) denotes a positive sign. The coordinate system shows the directions of the BF axes. Note that the HOMOs differ from one another only by a simple rotation.

as shown on Fig. 3, and we can use this molecule to demonstrate the effect discussed below Eq. (7), i.e., the absence of interference effects from randomly oriented molecules, when degenerate HOMOs differ only by a rotation. To this end we have compared the total harmonic yield with the yield from a single HOMO when the orientational distribution is as given by Eq. (16) and confirmed that the results agree except from an overall scaling factor. This is illustrated on Fig 4(a).

Next, we have carried out calculations of HHG from methane that has been one-dimensionally oriented with the BF z-axis at some fixed angle θ relative to the polarization direction. The orientational distribution used is given by Eq. (17). We do not show the harmonic spectrum in this case, since it does not differ much in structure from Fig. 4(a). This is probably due to the fact that methane is rather small and compact, which makes it spherical-like after χ-averaging. Consequently, no structure is revealed by the electrons, not even the most energetic, and the harmonics exhibit the same overall θ-dependence.

On Fig. 4(b) we show this typical angular dependence of the harmonics. In the figure the upper curve shows the signal when the coherence between the individual HOMOs is correctly accounted for [cf. Eq. (7)]. The other curves in the figure show the unphysical signals from each HOMO. Clearly, this figure illustrates that there is a strong interference between the single HOMO amplitudes in the angle resolved signal. We may understand the single HOMO signals in Fig. 4(b) from the structure of the

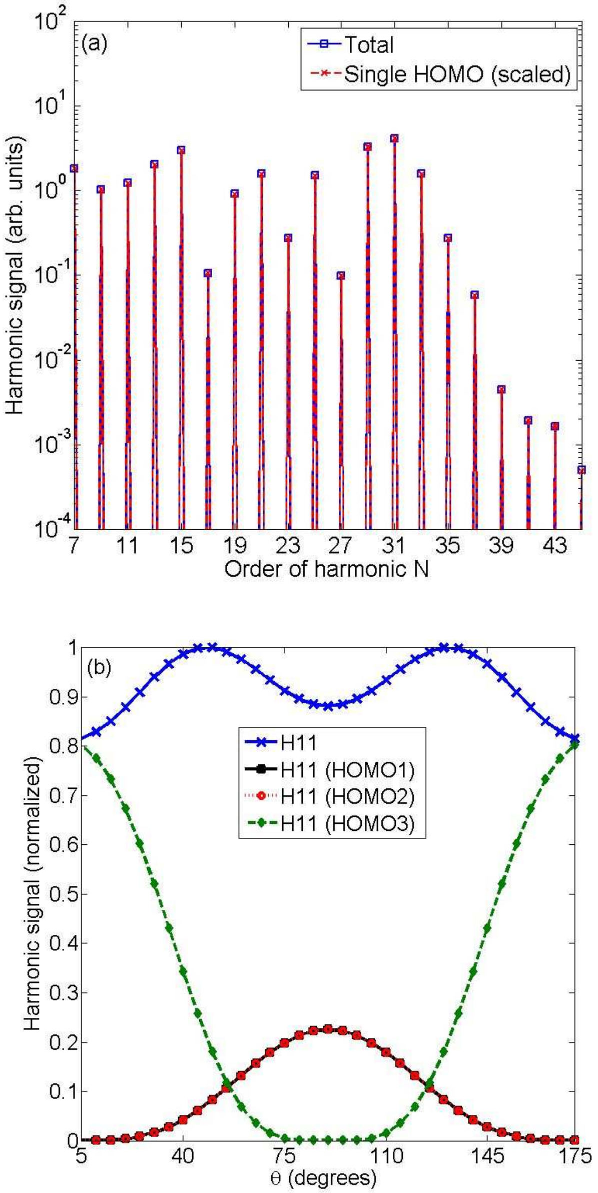

FIG. 4: (Color online) The figure illustrates the interference of high-harmonics coming from different orbitals as prescribed by Eq. (7). The physical system used is methane (CH_4). Panel (a) shows the total harmonic yield from randomly oriented methane. It is just a multiple of the harmonic yield from a single HOMO. Even harmonics vanish as a result of the orientational averaging. Panel (b) illustrates the detailed θ-dependence of the 11th harmonic (H11). Although not measurable, we also show the single HOMO signals. The calculated signals have all been normalized to the maximum total yield of the 11th harmonic. The figure underlines the importance of adding coherently the amplitude contributions from each HOMO, $\lambda = 1, 2, 3$.

HOMOs: First, we explain the dips. The vanishing signals of HOMO1 and HOMO2 at $\theta = 0°$ are explained by the fact that in this case the polarization vector points along the BF z-axis, hence coinciding with the nodal planes of these HOMOs, as seen from Fig. 3. Furthermore, the electron causing HHG must escape along the polarization axis to Eq. (13), and we conclude that these two HOMOs cannot generate harmonics for $\theta = 0°$. At $\theta = 90°$ the polarization axis is directed into the BF xy-plane which is the nodal plane of HOMO3 (see Fig. 3) and consequently HHG from HOMO3 is excluded. Second, we remark that the single HOMO-yield at a given value of θ is obtained by averaging amplitudes from all degrees of rotation around the BF z [cf.-axis (7) and (17)]. It is therefore obvious from symmetry that the results of HOMO1 and HOMO2 must be identical.

C. Propane and butane: Effects of orientation

In the following we consider propane (C_3H_8) and butane (C_4H_{10}). We begin with numerical results on the propane molecule. Figure 5 shows the HOMO of propane along with the harmonic signal in randomly oriented and one-dimensionally oriented scenarios corresponding to orientational distributions from Eqs. (16) and (17). The dependence of the HHG spectrum on orientation amounts to more than just a simple scaling, e.g., the 19th harmonic is alternately above and below the neighboring odd harmonics depending on the orientation of the propane molecule. We ascribe this to the fact that propane is a rather extended and open-structured molecule. In general, when the BF z-axis is close to the LF Z-axis the HHG is suppressed, because the almost vanishing wave function along the polarization direction [see Fig. 5(a)] makes the ATI amplitudes in Eq. (12) small. Notice also that the even harmonics disappear at an orientation of 90°. This is due to the fact that every photon absorption at this orientation changes the projection of the electron angular momentum on the Z-axis with $\pm\hbar$, and it is seen from Table I that an odd number of photon absorptions is necessary in order to start off and end up in the HOMO.

We remark that harmonics of order 15 to 27 are suppressed for $\theta = 90°$, which means that alignment is a tool for favorising the harmonics close to and above the semiclassical cutoff energy at $I_p + 3.17U_p \simeq 29 \times \hbar\omega$. These harmonics are known to be well phase-synchronized in the case of diatomic molecules [9], and this may also hold true in the case of propane. Furthermore, phase-synchronized harmonics are synchronically emitted and the superposition of such harmonics constitute the basis for the generation of attosecond pulses.

Figure 6 illustrates the HHG from butane. As with propane we observe a complicated behavior of the individual harmonics upon the orientation. Opposite to the case of propane, there is no particular orientation that favors harmonics near the semiclassical cutoff energy.

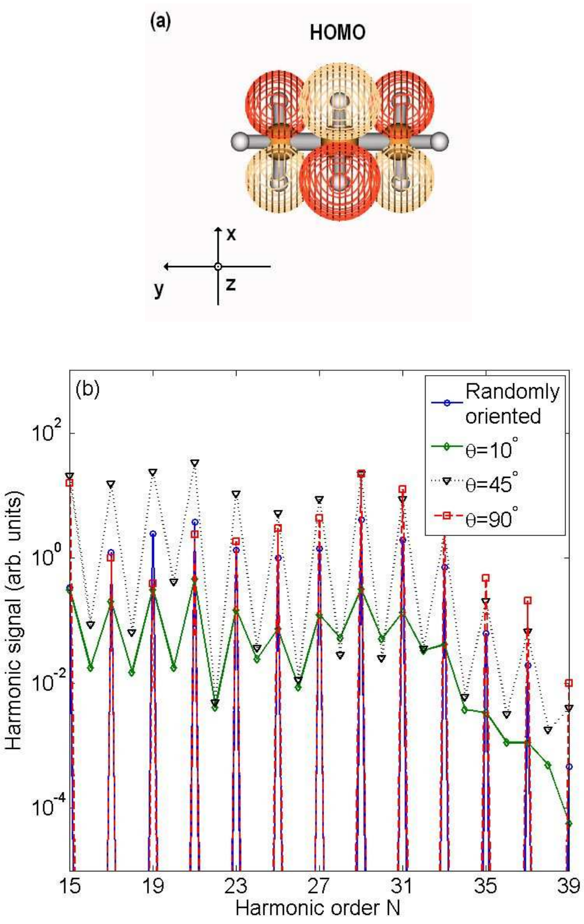

FIG. 5: (Color online) The figure clearly illustrates how the open and extended structure of propane leads to a harmonic spectrum with a complicated orientational dependence. Panel (a) shows the geometry of the propane molecule (C_3H_8) along with an isocontour of the HOMO. Dark shading (red online) denotes a negative sign of the HOMO wave function and light shading (brownish online) denotes a positive sign. The xyz-axes of the BF frame is shown. Panel (b) illustrates the dependence of the harmonic spectrum on the orientation of the propane molecule. At the orientation $\theta = 90^\circ$ even harmonics are suppressed as discussed in the text.

V. CONCLUSIONS AND OUTLOOK

In the present work we have discussed general issues related to the effects of molecular symmetry, degeneracy and orientation in HHG. To this end, we have considered the high-harmonic signal from several polyatomic molecules, namely ethylene, methane, propane and butane. In the case of ethylene we have shown how the dependence of orientation reflects the HOMO: The strength of the harmonics is increased when the laser polarization is directed away from the nodal plane, but the detailed orientational dependence differ from one harmonic to another. We have used methane as an example of a molecule with degenerate HOMOs. Then harmonic amplitudes of different HOMOs need to be added coherently, and interference effects are in general unavoidable. Although, some information about the individual HOMOs can be extracted by orienting the molecule we illustrated the importance of including all HOMOs when calculating the harmonic signal from one-dimensionally oriented methane. Finally, the propane and butane molecules served as illustrations of HHG from extended structures, and the individual harmonics carry their own characteristic orientational dependence. In the case of propane harmonics near the cutoff can be promoted by means of orientation and a selection of these energetic harmonics is of interest to attosecond pulse generation.

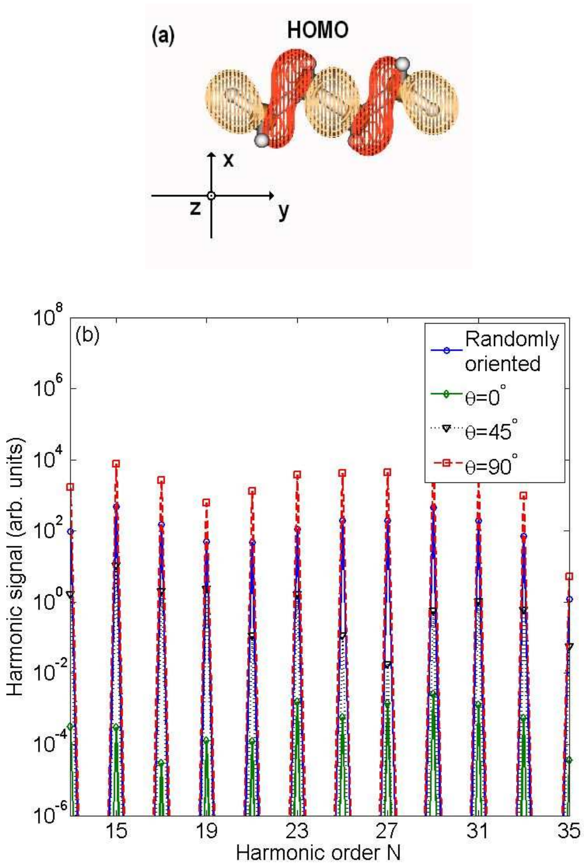

FIG. 6: (Color online) Panel (a) shows the geometry of the butane molecule (C_4H_{10}) and an isocontour of the HOMO. The sign of the HOMO wave function is indicated by the coloring, where dark shading (red online) denotes a negative sign and light shading (brownish online) denotes a positive sign. We also show the coordinate system of the BF frame. Panel (b) shows the harmonic spectrum corresponding to different orientations. As in the case of ethylene the HOMO is inversion symmetric which excludes the presence of even harmonics.

While we expect the conclusions drawn above to be fairly model independent we would like to mention a few open theoretical questions that should be addressed in the near future. In the present paper a relatively simple model using several approximations, including the strong-field approximation and a saddle-point approximation, has been applied to describe HHG. The model is formulated in length gauge, but at this level of approximation it is still to be settled wether another gauge would be more appropriate [25, 26]. In addition, a future challenge is to take into account the finite duration of the harmonic driving laserpulse. This is necessary in order to investigate further the possibility of using large molecules as sources of attosecond pulses.

Acknowledgments

The present work was supported by the Danish Research Agency (Grant. No. 2117-05-0081).

[1] G. Sansone, E. Benedetti, F. Calegari, C. Vozzi, L. Avaldi, R. Flammini, L. Poletto, P. Villoresi, C. Altucci, R. Velotta, et al., Science **314**, 443 (2006).

[2] J. J. Carrera, X. M. Tong, and S.-I. Chu, Phys. Rev. A **74**, 023404 (2006).

[3] W. Cao, P. Lu, P. Lan, W. Hong, and X. Wang, J. Phys. B **40**, 869 (2007).

[4] C. A. Haworth, L. E. Chipperfield, J. S. Robinson, P. L. Knight, J. P. Marangos, and J. W. G. Tisch, Nature Physics **3**, 52 (2007).

[5] J. Itatani, J. Levesque, D. Zeidler, H. Niikura, H. Pépin, J. C. Kieffer, P. B. Corkum, and D. M. Villeneuve, Nature (London) **432**, 867 (2004).

[6] R. Torres, N. Kajumba, J. G. Underwood, J. S. Robinson, S. Baker, J. W. G. Tisch, R. de Nalda, W. A. Bryan, R. Velotta, C. Altucci, et al., Phys. Rev. Lett. **98**, 203007 (2007).

[7] S. Patchkovskii, Z. Zhao, T. Brabec, and D. M. Villeneuve, J. Chem. Phys. **126**, 114306 (2007).

[8] C. Altucci, R. Velotta, E. Heesel, E. Springate, J. P. Marangos, C. Vozzi, E. Benedetti, F. Calegari, G. Sansone, S. Stagira, et al., Phys. Rev. A **73**, 043411 (2006).

[9] P. Lan, P. Lu, W. Cao, X. Wang, and G. Yang, Phys. Rev. A **74**, 063411 (2006).

[10] C. B. Madsen and L. B. Madsen, Phys. Rev. A **74**, 023403 (2006).

[11] B. Sundaram and P. W. Milonni, Phys. Rev. A **41**, 6571 (1990).

[12] K. Burnett, V. C. Reed, J. Cooper, and P. L. Knight, Phys. Rev. A **45**, 3347 (1992).

[13] C. B. Madsen, A. S. Mouritzen, T. K. Kjeldsen, and L. B. Madsen, arXiv:physics/0703234v1 (2007).

[14] R. N. Zare, *Angular momentum* (John Wiley & Sons, Inc., New York, 1988).

[15] H. Stapelfeldt and T. Seideman, Rev. Mod. Phys. **75**, 543 (2003).

[16] A. Rouzée, S. Guérin, V. Boudon, B. Lavorel, and O. Faucher, Phys. Rev. A **73**, 033418 (2006).

[17] J. G. Underwood, B. J. Sussman, and A. Stolow, Phys. Rev. Lett. **94**, 143002 (2005).

[18] M. Y. Kuchiev and V. N. Ostrovsky, Phys. Rev. A **60**, 3111 (1999).

[19] T. K. Kjeldsen, C. Z. Bisgaard, L. B. Madsen, and H. Stapelfeldt, Phys. Rev. A **71**, 013418 (2005).

[20] P. J. Linstrom and W. G. Mallard, *NIST Chemistry WebBook, NIST Standard Reference Database Number 69* (National Institute of Standards and Technology, Gaithersburg MD, 20899 (http://webbook.nist.gov), June 2005).

[21] M. W. Schmidt, K. K. Baldridge, J. A. Boatz, S. T. Elbert, M. S. Gordon, J. H. Jensen, S. Koseki, N. Matsunaga, K. A. Nguyen, S. Su, et al., Journal of Computational Chemistry **14**, 1347 (1993).

[22] E. Priori, G. Cerullo, M. Nisoli, S. Stagira, S. D. Silvestri, P. Villoresi, L. Poletto, P. Ceccherini, C. Altucci, R. Bruzzese, et al., Phys. Rev. A **61**, 063801 (2000).

[23] V. Tosa, E. Takahashi, Y. Nabekawa, and K. Midorikawa, Phys. Rev. A **67**, 063817 (2003).

[24] J. Levesque, D. Zeidler, J. P. Marangos, P. B. Corkum, and D. M. Villeneuve, Phys. Rev. Lett. **98**, 183903 (2007).

[25] C. C. Chirilă and M. Lein, Phys. Rev. A **73**, 023410 (2006).

[26] J. Chen and S. G. Chen, Phys. Rev. A **75**, 041402(R) (2007).